Quantitative biosensor detection by chemically exchanging hyperpolarized ^{129}Xe

Sergey Korchak,[a] Thomas Riemer,[b] Wolfgang Kilian,[a]
and Lorenz Mitschang[a]

[a]Physikalisch-Technische Bundesanstalt Braunschweig und Berlin
Division of Medical Physics and Metrological Information Technology
Abbestr. 2 – 12, 10587 Berlin, Germany
[b] University of Leipzig, Medical Department, Institute of Medical Physics and Biophysics,
Härtelstr. 16–18, 04107 Leipzig, Germany.Universität Leipzig

Supporting Information

Explicit functional form of $S(\rho,\tau)$

Free xenon magnetization density in solution $A(\rho)$.

The free xenon magnetization density in solution $A(\rho)$ is proportional to the product of the ^{129}Xe nuclear spin polarization P_{Xe}, the abundance of ^{129}Xe in the xenon gas r and the free xenon concentration in solution $\rho = s\ p$, where s denotes the xenon solubility and p the xenon partial pressure in the gas mixture bubbled through the solution to achieve xenon saturation. While ρ and r are well defined within this work (natural abundant ^{129}Xe, aqueous solution – see Table 1), the polarization of the ^{129}Xe atoms is the result of various processes relevant to the spin-exchange optical pumping (SEOP) in the polarizer. As shown in Fig. S1, experimental data nonetheless suggest a smooth dependence of P_{Xe} on the xenon partial pressure such that a rather simple, analytical function could be possibly derived for $A(\rho)$ which would suffice for the establishment of the explicit model $S(\rho,\tau)$. We emphasize thus not to aim at an exhaustive description of the physics involved in SEOP but to motivate a functional form for $A(\rho)$ by referring to the pertinent studies in the field.[28-30]

Even though still being a topic of research[28] there is a common description of the ^{129}Xe polarization achieved in an optical cell by SEOP as given by

$$P_{Xe} = \langle P_{Rb} \rangle \frac{\gamma_{SE}}{\gamma_{SE} + \Gamma_1}\left(1 - \exp\left\{-\tau_{res}\left(\gamma_{SE} + \Gamma_1\right)\right\}\right) \qquad [S1]$$

where $\langle P_{Rb} \rangle$ is the average Rubidium electron polarization, γ_{SE} is the spin-exchange rate characterizing the efficiency of polarization transfer from rubidium electrons to ^{129}Xe nuclei, Γ_1 is the ^{129}Xe nuclear spin relaxation rate, and τ_{res} is the residence time of a xenon atom in the optical pumping cell. To disentangle the effects on P_{Xe} by a variation of the xenon partial pressure in a gas mixture with nitrogen and helium as quenching and buffer gas, respectively, we take the known specifics of our polarizer into account. The total gas flow ($\tau_{res} \approx 4$ minutes) as well as the total gas pressure p_{tot} are kept constant while the partial pressures of helium and xenon are set complementarily (p_{tot} = 3 bar, p_{N2} = 0.2 bar, p_{He} = 2.8 bar - p_{Xe},

taken at room temperature as absolute pressures). The xenon polarization build-up time $(\gamma_{\mathrm{SE}}+\Gamma_1)^{-1}$ can be straightaway determined by xenon inversion recovery during SEOP using an online NMR setup.[30,44] We found built-up times in the order three minutes for our polarizer. As our optical pumping cell is only partly sitting within a temperature controlled oven[44] it is not possible to assign a single temperature to the SEOP cell and thus to calculate the rubidium number density by one of the well-known vapor pressure curves. However, homogenization due to strong gas convection should facilitate the assignment of a mean rubidium number density to the SEOP process.[30]

In principle, each of the factors $\langle P_{\mathrm{Rb}}\rangle$, γ_{SE} and Γ_1 contributes to the dependency of P_{Xe} on the xenon partial pressure:

- The Rubidium polarization in a SEOP-cell

$$P_{Rb}(z)=\frac{\gamma_{OP}(z)}{\gamma_{OP}(z)+\Gamma_{SD}} \qquad [S2]$$

$$\Gamma_{SD}=\sum_i [G_i]\kappa_{SD}^{Rb-i}$$

varies with p_{Xe} via the alkali-metal spin-destruction rate which is strongly dependent on the various buffer-gas densities $[G_{\mathrm{i}}]$ by way of the corresponding spin-destruction cross sections κ_{SD}^{Rb-i}. As shown in Table I in Ref. 29, xenon itself is the most potent Rb-spin destroyer with a spin-destruction cross section about four orders of magnitude larger than the ones for helium and nitrogen. In contrast, the optical pumping rate $\gamma_{\mathrm{OP}}(z)$ (the overlap of the frequency- and position-dependent laser intensity and the alkali-metal absorption cross section) is constant for a given laser power and for constant rubidium density [Rb], as is the case here. Potential Rb relaxation due to radiation trapping as well as spin-rotation interactionis neglected in comparison to Γ_{SD} due to the use of nitrogen as fluorescent quenching gas and nitrogen and helium as agents for the breakup of Rb-Xe van der Waals dimers.[30] It should be noted that for the high-power laser diodes nowadays used in SEOP polarizers unity rubidium polarization can be reached at vanishing xenon partial pressure.

- The xenon-rubidium spin-exchange rate γ_{SE} has contributions from binary collisions with the pressure independent rate coefficient κ_{SE}^{BC}, and persistent-dimer (van der Waals) collisions showing a rate coefficient decaying inversely proportional to the various gas densities[29]

$$\gamma_{SE}=[Rb]\kappa_{SE}^{BC}+\frac{[Rb]}{\frac{[Xe]}{\xi_{Xe}}+\frac{[N2]}{\xi_{N2}}+\frac{[He]}{\xi_{He}}}=[Rb]\left(\kappa_{SE}^{Rb-Xe}+\frac{\xi_{Xe}}{[Xe]}\frac{1}{1+\frac{\xi_{Xe}[N2]}{\xi_{N2}[Xe]}+\frac{\xi_{Xe}[He]}{\xi_{He}[Xe]}}\right) \qquad [S3]$$

Using $\xi_{Xe}=5230$ $\mathrm{s^{-1}}$, $\xi_{N2}=5700$ $\mathrm{s^{-1}}$, $\xi_{He}=17000$ $\mathrm{s^{-1}}$ and $\kappa_{SE}^{BC}=2.17\times10^{-16}$ $\mathrm{cm^3 s^{-1}}$ (from Ref. 29), $\gamma_{\mathrm{SE}}/[\mathrm{Rb}]$ is calculated to lie within 4.7 and 3.8×10^{-16} $\mathrm{cm^3 s^{-1}}$ for our gas mixture with xenon partial pressures from 0.01 to 0.8 bar, respectively.

- The xenon relaxation rate Γ_1 is governed by intrinsic (gas phase collisions) and extrinsic (wall collisions, magnetic field gradients) relaxation mechanisms with the latter unaffected by changes in the gas composition. The gas phase collisions, however, are again of either the binary or the persistent-dimer kind. Both mechanisms are surely dependent on the gas composition, particularly the xenon density, but induce relaxation times in the order of hours which are irrelevant in view of the relaxation rate by extrinsic mechanisms. Thus, the relaxation of hyperpolarized xenon in our polarizer should not be affected by variations in the xenon partial pressure.

We probed the maximum achievable xenon polarization to be approximately $P_0 \approx 0.25$ by running our polarizer at only $p_{Xe} = 0.01$ bar (see Fig. S1). With $\langle P_{Rb} \rangle$ reaching unity for vanishing xenon density, one obtains from the limiting expression for $P_{Xe}(p_{Xe} \rightarrow 0)$ set to 0.25 and the built-up time $(\gamma_{SE} + \Gamma_1)^{-1}$ set to 3 minutes estimates $\Gamma_1 \approx 0.004$ s^{-1} and $\gamma_{SE}(p_{Xe} \rightarrow 0) \approx 0.002$ s^{-1}. Taking the latter value together with 4.7×10^{-16} cm^{3}s^{-1} for γ_{SE}/[Rb] at vanishing p_{Xe} (see Eq. S3), the mean rubidium number-density becomes 4.3×10^{12} cm^{-3}. The factor $\gamma_{SE}/(\gamma_{SE}+\Gamma_1)$ in Eq. S1 is thus estimated to drop from 0.25 to 0.22, or by about 12%, for a variation of the xenon partial pressure from 0.01 to 0.8 bar as used in our experiments. This is a small effect in comparison to the overall drop of the xenon polarization P_{Xe} over the same pressure range of nearly 90 %. We thus neglect the slowly varying contribution against the fast one, and approximate P_{Xe} in its dependence on the xenon pressure to be governed by the mean rubidium polarization $\langle P_{Rb} \rangle$. Eq. S1 then simplifies to

$$P \propto P_0 \frac{1}{1+\alpha p} \qquad \text{[S4]}$$

with the parameter α reflecting the dependence of the xenon polarization on the xenon partial pressure effectively. Thus, the magnetization density in a solution saturated at xenon partial pressure p and of xenon concentration $\rho = s\ p$ is proportional to

$$A(\rho) = \frac{rP_0\rho}{1+\alpha\rho/s} \qquad \text{[S5]}$$

which is the basic signal intensity used in the model $S(\rho,\tau)$ for the Hyper-CEST effect. The constant parameters r and P_0 are absorbed in the global scaling factor for $S(\rho,\tau)$ when the model is applied to experimental data and do therefore not appear in the explicit function of $S(\rho,\tau)$ in the main text. Experimental xenon polarization data from our polarizer could be fitted well by Eq. S4 with $\alpha = 8.36 \pm 0.76$ bar^{-1} (Fig. S1).

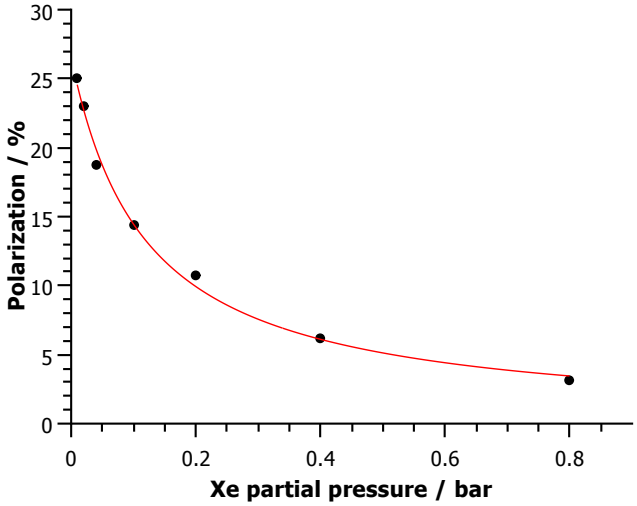

Fig. S1. Polarization of hpXe in dependence of xenon partial pressure in the gas mixture being fed through the polarizer and into the solution. The experimental data (black dots) are the MR signal intensities of the freely dissolved xenon signal (196 ppm) divided by the xenon partial pressure and normalized to the maximum polarization $P_0 = 0.25$ we get at very low xenon pressure[44]. The red line is a non-linear least-squares fit of Eq. S4 to the data for the parameter estimation α = 8.36±0.76 bar^{-1}.

Complex formation rate $k_{on}(\rho)$. The exchange kinetics in the CrA-hpXe host-guest system is governed by dissociative and degenerate exchange reactions[8,19] with the rate for complex formation given by[34]

$$k_{on}(\rho) = (c + k\,\rho)\frac{K\,C}{1 + K\,\rho} \quad . \qquad \text{[S6]}$$

The first factor $k_{off} = c + k\rho$ is the rate for breakup of the complex caused by dissociative processes with the rate coefficient c as well as by the free xenon concentration driven degenerate exchange with the rate coefficient k. The second factor is the ratio of the concentration of xenon occupied host molecules to the concentration of free xenon where C denotes the total host concentration and K is the complex association constant.

Position ρ_{max}, τ_{max} of maximum Hyper-CEST effect

In general, for any given free xenon concentration ρ the irradiation period τ_{max} for maximum Hyper-CEST effect renders the partial derivative $\partial S(\rho,\tau)/\partial\tau$ vanishing. This occurs when

$$\tau_{\max} = \ln\left[1 + k_{on}(\rho)/R\right]/k_{on}(\rho), \qquad \text{[S7]}$$

an expression found previously in an optimization of the RF saturation process but extended here for the dependence on the free xenon concentration.[49] The optimum τ_{max} changes with the total host concentration which is linearly related to $k_{on}(\rho)$ as shown above. The crest line of the maximum Hyper-CEST effect for any choice of ρ is given explicitly by $S(\rho, \tau_{max}(\rho))$ (Figs. 1C, S4). Viewed as a one-dimensional function of the variable ρ, the position of the single maximum $\rho_{\max}$ which is also the ρ-coordinate of the maximum of the two-dimensional function $S(\rho, \tau)$ can now be determined conveniently. Despite $S(\rho, \tau_{max}(\rho))$ being analytical, we could determine ρ_{max} for finite C only numerically by nested intervals. The optimum saturation period can then be obtained by the evaluation of the expression for τ_{max} at ρ_{max}.

For vanishing host concentration, however, $S(\rho, \tau)$ may be approximated by linear expansion in C. The partial derivatives with respect to ρ and τ now vanish for the settings

$$\rho_{max} = \frac{k + \sqrt{k^2 + c(\alpha cK - \alpha k - kK)}}{\alpha cK - \alpha k - kK}, \text{ and } \tau_{max} = \frac{1}{R}, \qquad \text{[S8]}$$

explaining the existence and the location of a unique converging point of the maxima loci for vanishing host concentration.

As pointed out in the the main text (discussion section), the model requires extension in case of incomplete RF saturation by the replacement $k_{on} \to k_{on} \cdot f(\omega, \rho)$ in Eq. 1 with the factor $f(\omega,\rho) = \omega^2/(\omega^2 + k_{off}(\rho)^2)$, and with ω for the saturation power in units of xenon angular frequency. The maximum position at τ_{max} and ρ_{max} is still determined by Eq. S7 above and the maximum position of the crest line $S(\rho, \tau_{max}(\rho))$, respectively, provided the replacement $k_{on} \to k_{on} \cdot f(\omega, \rho)$ is also taken into account. However, we could not derive an analytical expression for ρ_{max} in the limit of vanishing C for incomplete saturation.

Binding constant for CrA-xenon complex formation

Free CrA in aqueous solution is known to have a fluorescence response with maximum at 323 nm for excitation by UV-light which, however, is quenched by the binding of small guest molecules, like xenon or N_2.[32] Observing the CrA-fluorescence while modulating the various gas concentrations will thus indicate respective effective binding constants.

We first wanted to find out whether He, the most concentrated gas in the stream from the polarizer, could be ignored as a binding partner for CrA due to its smallness and inertness. For a CrA in water solution saturated with xenon at constant partial pressure of 5 mbar and a variable admixture of He of up to 3 bar we did not find any changes in the fluorescence.

We then assumed xenon (Xe) and water (W) to bind competitively with association constants K^{Xe} and K^{W}, respectively, to CrA in binary reactions. The fluorescence is modeled to be proportional to the total concentration of CrA with contributions from empty cage, $[C]$, and complexes with xenon, $[CXe]$, or water, $[CW]$

$$a\cdot[C]+b\cdot[CXe]+c\cdot[CW]=\alpha+\frac{\beta}{1+K_{eff}^{Xe}[Xe]} \qquad [S9]$$

where a, b, c, α, and β are constants, $[Xe]$ is the concentrations of free xenon, and $K_{eff}^{Xe}=K^{Xe}/(1+K^{W}[W])$ is the effective binding constant for xenon in aqueous solution with $[W]$ for the free water concentration.

In Fig. S2 binding curves according to Eq. S9 are shown for CrA and xenon in water at the two temperatures of 298 K and 310 K. The xenon concentration was varied by the addition of the xenon (together with a constant admixture of 0.5 bar He as carrier gas) to the solution and shacking for dissolution and saturation ([Xe] = $s\,p$ by Henry's law for xenon partial pressure p and solubility s=4.32 mM/bar at 298 K or s=3.25 mM/bar at 310 K, respectively). Non-linear least-squares fits of Eq. S9 to the data gave $K_{eff}^{X}=69100\pm2700\ \mathrm{M^{-1}}$ and $K_{eff}^{X}=34800\pm600\ \mathrm{M^{-1}}$ at 298 K and 310 K, respectively.

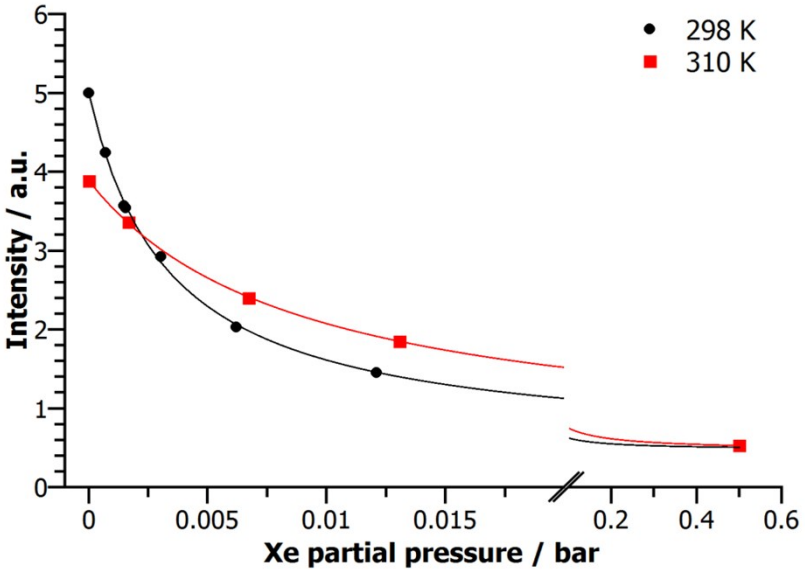

Fig. S2. Fluorescence amplitude at 323 nm for CrA and xenon in water in dependence of xenon partial pressure at 298 K (black dots) and 310 K (red squares) with fits (lines) of the function in Eq. S9.

In a similar manner, by varying N_2 in between 0.5 to 3 bar in a gas mixture with xenon at constantly 3 mbar, the effective binding constant for N_2 in a water solution with CrA was determined as $K_{eff}^{N_2} = 1420 \pm 110\,\mathrm{M}^{-1}$ and $K_{eff}^{N_2} = 1830 \pm 590\,\mathrm{M}^{-1}$ at 298 K and 310 K.

In our experimental setup the hyperpolarized xenon was always delivered together with constantly 0.2 bar N_2 and a variable amount of up to 2.79 bar helium to the CrA in water solution. While the binding of helium to CrA is negligible (see above), the competition of xenon, N_2 and water for the host can be described by the extension of Eq. S9 by contributions to the fluorescence proportional to the concentrations of the CrA-N_2 complex, $[CN_2]$, and of the free nitrogen, $[N_2]$,

$$a \cdot [C] + b \cdot [CXe] + c \cdot [CW] + d \cdot [CN_2] = \alpha + \frac{\beta}{1 + K_{eff}^{Xe}[Xe]/(1 + K_{eff}^{N_2}[N_2])} \,. \qquad \text{[S10]}$$

The binding constant of xenon to CrA in water in the presence of N_2 is thus $K_{eff}^{Xe}[Xe]/(1 + K_{eff}^{N_2}[N_2])$ and becomes 58400±6800 M^{-1} at 298 K and 28900±2200 M^{-1} at 310 K, respectively, using the specifications derived above and a nitrogen solubility in water of 0.655 Mbar^{-1} at 298 K and of 0.567 Mbar^{-1} at 310 K, respectively.[42] The uncertainties are error propagations of the uncertainties in K_{eff}^{Xe} and $K_{eff}^{N_2}$.

Rate coefficients of the exchange kinetics at 310 K

One-dimensional exchange spectroscopy in combination with variation of xenon partial pressure was used to determine the rate coefficients c and k for xenon reversibly binding to CrA. Consider a solution of CrA and hyperpolarized xenon with the magnetization M_{XE} in the pool of freely dissolved xenon selectively inverted and subsequently allowed to exchange freely with the host before, again by a selective pulse, the magnetization of host-bound xenon M_H is excited and acquired (for details of the experiment see Ref. 34). The rate coefficient for the magnetization exchange in between both pools is the sum of the complex formation and dissociation rates, $k_{off}+ k_{on}$, which may be written

$$k_{on} + k_{off} = (c + k\,\rho)\left\{1 + \frac{K\,C}{1 + K\,\rho}\right\} \qquad [S11]$$

using the relation for k_{on} in Eq. S5.

A solution of total host concentration C=11 μM was saturated by gas bubbling with hyperpolarized xenon for different settings of the xenon partial pressure p such that a free xenon concentration of $\rho = s\,p$ prevailed for xenon solubility s=3.25 mM/bar at 310 K in each case according to Henry's law. For variation of the exchange period the decay of host-bound magnetization due to replacement by inverted free xenon magnetization was monitored by the signal intensity. The decay rate $R_d = k_{off}+k_{on}$ was determined by fitting a mono-exponential function to the signal intensities in dependence of the exchange period. A contribution to R_d by relaxation in the mHz range is here neglected.[34] The rates R_d are displayed in Fig. S3 in dependence of the various xenon partial pressure settings.

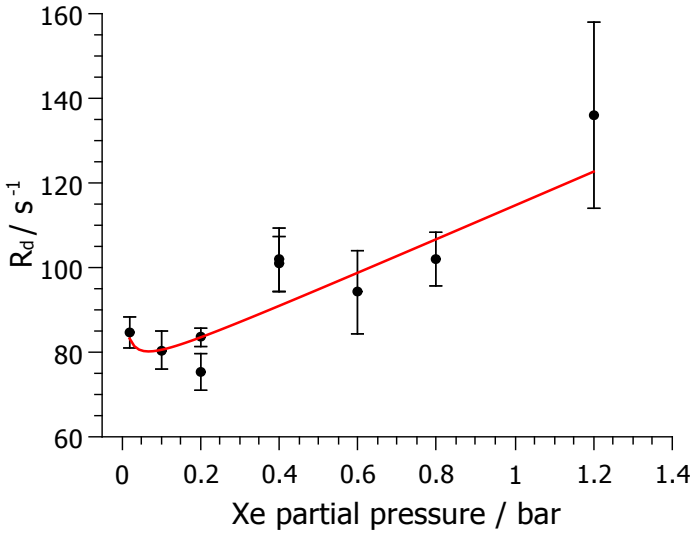

Fig. S3. Decay rates of caged xenon in dependence of xenon partial pressure (black dots, error margins are the standard error in fitting the rates) and fit of Eq. S10 (red line).

For known binding constant K = 28900 M^{-1} at 310 K (derived above) and total host concentration C=11 μM the exchange rate coefficients with uncertainties c = 74.1 ± 2.5 s^{-1} and k = 12400 ± 2600 $M^{-1}s^{-1}$ were determined by fitting of Eq. S11 to the data.

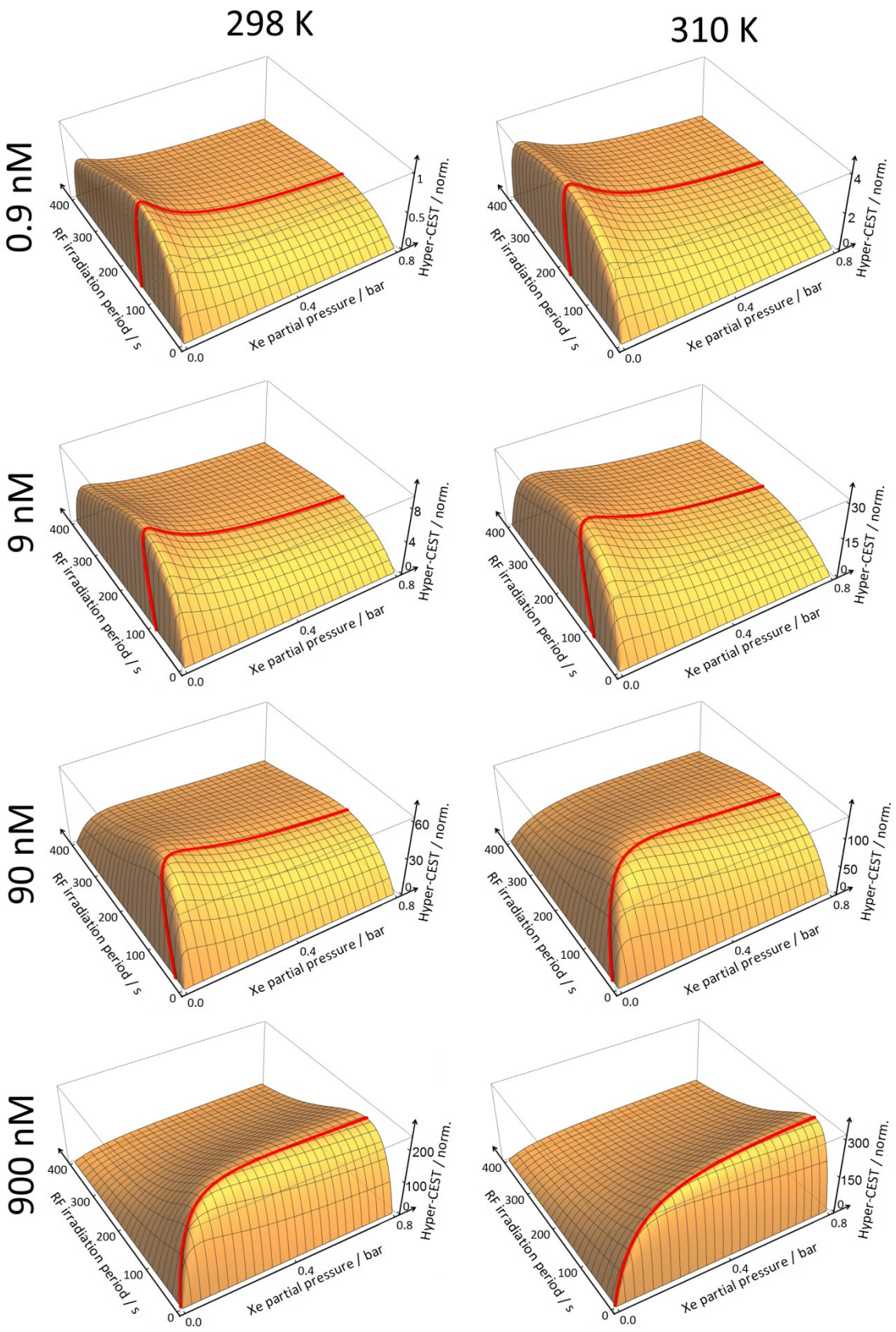

Fig. S4. Evaluations of the model for the Hyper-CEST effect at temperatures 298 K and 310 K, and for aqueous solutions of CrA of 0.9 nM, 9 nM, 90 nM, and 900 nM, respectively. The model parameters from Table 1 in the main text were used. The amplitudes are normalized to the maximum effect for 0.9 nM CrA-concentration at 298 K (also used in Figs. 1C and 2A in the main text).